Mechanical Properties of Multi-walled Beryllium-Oxide Nanotubes: A molecular Dynamics Simulation Study

Yaser Rostamiyan
Islamic Azad University Sari Branch
Navid Shahab
Islamic Azad University Sari Branch
Christos Spitas
Nazarbayev University
Amin Hamed Mashhadzadeh (amin.hamed.m@gmail.com)
Nazarbayev University https://orcid.org/0000-0001-8146-8198

Research Article

Keywords: Molecular dynamics, Beryllium-Oxide nanotube, Young's modulus, multi-walled nanotube

Posted Date: May 23rd, 2022

DOI: https://doi.org/10.21203/rs.3.rs-1406814/v1

Abstract

Molecular Dynamic (MD) simulation was employed to take the molecular fingerprint of mechanical properties of Beryllium-Oxide nanotubes (BeONTs). In this regard, the effect of the radius, the number of walls (single-, double- and triple-walled), and interlayer distance, as well as temperature on the Young's modulus, failure stress and failure strain are visualized and discussed. It was unveiled that larger single-walled BeONTs have lower Young's modulus in zigzag and armchair direction, and the highest Young's modulus were obtained for the (8,0) zigzag and (4,4) armchair SWBeONTs as of 645.71GPa and 624.81GPa, respectively. Unlike Young's modulus, however, the failure properties of the armchair structures were higher than those of zigzag ones. Furthermore, similar to SWBEONTs, an increase in the interlayer distance of double-walled BeONTs (DWBeONTs) led to a slight reduction in Young's modulus value, while no meaningful trend was found among failure behavior. For double-walled BeONTs (TWBeONTs), the elastic modulus was obviously higher in both armchair and zigzag directions compared to DWBeONTs.

1. Introduction

Non-carbon nanotubes, also called inorganic nanotubes, are a class of nanomaterials that have recently been widely considered by the researchers, similar to carbon nanotubes, due to their outstanding mechanical, optical, thermal, and electronic properties. These nanostructures mainly include metal-oxide nanotubes such as Zinc-Oxide (ZnO), Beryllium-Oxide (BeO), and Titanium-Oxide (TiO_2), nitride-based nanotubes such as Boron-nitride (BN), Aluminum-nitride (AlN), Gallium-nitride (GaN), and also nanotubes composed of the elements of group VI periodic table such as silicon-carbide (SiC) and silicon-germanium (SiGe), widely considered in both theoretical and experimental research studies [1–7]. However, since the experimental approaches usually compel a high amount of expenditure on the research projects, theoretical studies have become more popular over the past few decades.

Ab-initio based density functional theory (DFT) and molecular dynamic (MD) simulation are the most used theoretical techniques in investigating the properties of nanotube structures and the results of these methods have been reported to be close to those of experimental data [8, 9]. In this regard, Jun-Hua et al. investigated the mechanical properties of AlN nanotubes with both zigzag and armchair chirality's using DFT and found that an increase in the diameter of both types of AlNNTs resulted in higher Young's modulus as well as band gap energy [10]. Cong et al. studied the mechanical properties of different Boron-nitride/Aluminum nanocomposite by the employment of MD simulations. They reported that higher Young's modulus, yield strain, and yield stress were obtained in nanotubes with higher diameters [11]. Liu et.al combined MD and DFT to probe the properties of single-walled SiGeNTs with zigzag and armchair chirality and reported that nanotubes with larger dimensions were more stable structures than those with smaller dimensions[12]. In a DFT study, ZnO nanotube was compared with the ZnO sheet with their adsorption properties by Mashahdzadeh and coworkers. They found that ZnO showed better adsorption capacity in nanotube form compared to sheet form [13].

Beryllium oxide (BeO) is a semiconducting oxide which its graphene form was firstly introduced by Contineza in the 1990s [14]. This nanostructure exhibits considerable properties such as high electrical resistivity, outstanding thermal conductivity, acceptable energy storage capability, and good hardness so that it has

recently become a subject of many research studies [15–18]. Sorokin et al. made a comparison between the properties of BeO nanotubes and BeO graphene-like structures trough a DFT research work. They found higher stability of these structures compared to single BeO molecules [19]. In another DFT-based study, Fathalian et al. considered the H_2 adsorption properties of zigzag BeONTs and showed these nanotubes would be suitable candidates for this purpose [20]. In addition to single nanotubes, the properties of some other nanostructures developed from these nanotubes including multi-walled, functionalized, doped and defective structures have also been attractive for researchers. Anota et al. employed the DFT method to find out the effect of functionalization on the electronic behavior of BeONTs which were functionalized by the hydroxyl (-OH) group and found that the semiconducting properties of nanotubes remained almost unchanged after functionalization [21].

Fereidoon et.al considered Young's modulus of zigzag and armchair one, two and three wall Boron-Nitride nanotubes (BNNTs) versus the number of walls using molecular dynamic (MD) simulations and found higher moduli versus adding more walls to the nanotube [22]. In a defect investigation work, Andressa et al. used the DFT technique for considering the effect of vacancy defects on the electronic levels of Boron-nitride nanotubes and showed that vacancies could improve the electronic levels of this nanotube and make it an appropriate choice for adsorbing H_2 molecules [23]. MD was employed in another study by Yang et al. to consider the fracture mechanism of single-walled CNT under vacancy and Stone-Wales defects. Their results demonstrated that Stone-Wales defects showed lower stress concentration compared to vacancy defects [24].

In a previous work, we studied mechanical properties of multi-walled beryllium oxide (BeO) nanotubes and nanopeapods using DFT computations [18]. However, DFT outcomes are just mathematical outcomes based on modulus performed at absolute temperature. To capture other mechanical properties as a function of time as well as to pattern fracture behavior in a scale which is close to the real case in a computationally cost effective manner, one needs to use MD simulation [25, 26]. Moreover, mechanical properties of nanotubes are severely depended on their length, which can be imaged in MD computational analysis [27]. Herein we used MD simulation to study the effect of diameter, temperature and the number of walls and on mechanical behavior of multi-walled BeO nanotubes in armchair and zigzag chirality. The Young's modulus, failure stress, and failure strain of one-, two- and three-walled BeO nanotubes were modeled and discussed at constant and variable temperature.

2. Computational Section

Molecular dynamic (MD) technique which is based on Newton's second law using classical mechanics [28], was applied in this article to consider the mechanical properties of the armchair and zigzag one, two, and three wall BeONTs. Large-Scale Atomic/Molecular Massively Parallel Simulator (LAMMPS) was employed to model the under evaluation nanostructures as well as considering the Long-range Coulomb atomic interactions. MD is able to provide scalable codes so, it makes LAMMPS act on parallel platforms efficiently [29]. Visual Molecular Dynamics (VMD) indicator was selected to analyze the results obtained from simulation due to being an appropriate tool for supporting various formats and outputs particularly those obtained from LAMMPS. Selecting a suitable potential function is a critical factor for simulating through MD because this function directly affects the precision of the results. In this work, classical multi-body Tersoff

potential was used to define the interactions among the elements of the simulated systems [30]. Since the interactions defined by Tersoff are based on the bond orders so, this potential function is suitable for determining different bond states of atoms using the same parameters [30]. Furthermore, periodic boundary conditions which should be applied along the axial direction by the employment of isothermal-isobaric ensemble (NPT). The temperature varied between 300°K and 1000°K for all single-walled structures and was set to 300°K for multi-walled and defective ones. Besides, the pressure was set to 1bar and we also applied Non-equilibrium simulation mode to allow the ends of the BeONTs to move along the loading direction at a predefined at a consistent strain rate. In some of the previous studies, the most acceptable results were achieved when the time step was between 0.5–0.8 fs and in other studies this variable was adjusted between 0.1 and 1 fs for uniaxial tensile tests [28, 31]. To perform tensile tests by MD simulations, strain should be applied to the nanotubes at a constant rate and, as far as we know, the failure of the under loading structure is related to the strain rate so, lower strain rates provide the system enough time to be relaxed [32]. Since the strain rates in the range of 0.0005 Ps^{-1} and 0.01 Ps^{-1} have extensively been employed in MD research studies [22, 27], we selected strain rate and time step equal to 0.01 Ps^{-1} and 1fs respectively. To consider the mechanical behavior, different single-walled, multi-walled, and defective BeONTs were put under uniaxial tensile loading to obtain stress-strain evaluation plots and the stress-strain relation was used to calculate the failure stress, failure strain and Young's modulus of all simulated BeO nanotubes.

3. Results And Discussion

a. Geometrical design

To investigate the mechanical behavior of one, two and three wall BeONTs all zigzag and armchair samples were designed under the MD framework. Figure 1 presents a schematic of the simulated nanotubes studied in the current article and Table 1 includes all of the structures that were simulated along with their number of atoms. The average Be-O bond length was obtained equal to 1.57Å and 1.58Å for the zigzag and armchair structures respectively which are in good accordance with the results of the earlier studies [33–36].

Table 1
Stoichiometry of SWBeONTs, DWBeONTs and TWBeONTs.

Chirality	Number of Atoms
(4,4) SWBeONT	352
(6,6) SWBeONT	528
(8,8) SWBeONT	704
(10,10) SWBeONT	880
(12,12) SWBeONT	1056
(8,0) SWBeONT	384
(10,0) SWBeONT	480
(12,0) SWBeONT	576
(14,0) SWBeONT	672
(16,0) SWBeONT	768
(18,0) SWBeONT	864
(20,0) SWBeONT	960
(4,4)@(8,8) DWBeONTs	1056
(4,4)@(9,9) DWBeONTs	1144
(4,4)@(10,10) DWBeONTs	1232
(8,0)@(14,0) DWBeONTs	1056
(8,0)@(15,0) DWBeONTs	1104
(8,0)@(16,0) DWBeONTs	1152
(8,0)@(18,0) DWBeONTs	1248
(4,4)@(8,8)@(12,12) TWBeONT	2112
(8,0)@(14,0)@(20,0) TWBeONT	2016

Table 2
Mechanical properties of armchair SWBeONTs under uniaxial tensile tests at 300°K.

Chirality	**(4,4)**	**(6,6)**	**(8,8)**	**(10,10)**	**(12,12)**
Young's Modulus	624.81	619.21	613.48	605.09	583.09
Failure Stress	101.62	101.37	102.42	100.86	102.40
Failure Strain	0.247	0.250	0.252	0.255	0.256

Table 3
Mechanical properties of zigzag SWBeONTs under uniaxial tensile tests at 300°K.

Chirality	**(8,0)**	**(10,0)**	**(12,0)**	**(14,0)**	**(16,0)**	**(18,0)**	**(20,0)**
Young's Modulus	645.71	631.92	621.02	617.13	605.82	591.83	587.86
Failure Stress	83.60	82.55	82.58	82.25	82.13	81.55	83.12
Failure Strain	0.192	0.189	0.186	0.186	0.185	0.182	0.182

Table 4
Effect of temperature on mechanical properties of zigzag (18,0) and armchair (10,10).

Chirality	Mechanical Properties	Temperature (°K)							
		300	400	500	600	700	800	900	1000
(18,0)	Young's Modulus (GPa)	591.83	586.90	579.02	563.03	554.23	546.27	526.30	507.89
	Failure Stress (GPa)	79.55	77.08	74.03	70.77	68.60	65.82	64.44	56.73
	Failure Strain	0.182	0.172	0.162	0.154	0.152	0.146	0.141	0.117
(10,10)	Young's Modulus (GPa)	605.09	590.25	585.73	579.00	573.39	544.89	536.66	528.64
	Failure Stress (GPa)	99.86	95.51	92.85	90.74	83.70	78.97	68.85	66.67
	Failure Strain	0.255	0.229	0.220	0.214	0.189	0.180	0.153	0.149

b. Mechanical properties of single-walled BeONTs

Concerning the mechanical properties of single-walled BeO nanotubes, seven zigzag nanotube including structures (8,0), (10,0), (12,0), (14,0), (16,0), (18,0), and (20,0) and five armchair structures including (4,4), (6,6), (8,8), (10,10), and (12,12) were simulated using MD. To calculate Young's modulus, we put all samples under uniaxial tensile loading and stress-strain curves were plotted accordingly. A schematic of a double-walled nanotube under tensile loading is presented in Fig. 2, and Fig. 3a shows the a stress-strain curve which is plotted for zigzag structure (8,0). As seen, the stress-strain relation is not linear so, to calculate young's modulus, we fitted a second-order polynomial to the linear part of the stress-strain plot regarding Fig. 3b. The elastic modulus was calculated through the following equation:

$$\sigma = \frac{\partial U}{\partial \varepsilon} = D\varepsilon^2 + E\varepsilon + C \qquad (1)$$

1.1. Mechanical properties of double-walled BeONTs

At this stage we modeled four zigzag double-walled structures including (8,0)@(14,0), (8,0)@(15,0,), (8,0)@(16,0), and (8,0)@(17,0) and three armchair structures including (4,4)@(8,8), (4,4)@(9,9), and (4,4)@(10,10) as shown in Fig. 7. Interlayer distance has undoubtedly increased with an increase in the based nanotubes' radius. As well as the previous section, all double-walled structures were put under uniaxial tensile loading and the obtained results are illustrated in Fig. 8, Table 5 and Table 6. Regarding Fig. 8, we can see that armchair and zigzag structures revealed contradictory behavior via interlayer distance. Similar to single-walled structures Young's modulus of zigzag DWBeONTs generally reduced (except one point) via an increase in the interlayer distance while this property rose constantly via the increase in interlayer distance of the armchair structures. The highest calculated values of Young's modulus belonged to (8,0)@(15,0,) zigzag and (4,4)@(10,10) armchair DWBeONTs with the magnitudes of 659.75GPa and 640.67GPa respectively. In an MD theoretical approach Fereidoon et l. found a reduction in Young's modulus of both armchair and zigzag DWBNNTs via interlayer distance rising [15]. Furthermore, the failure properties of the zigzag double-walled structures did not show a significant trend as well as single-walled ones while the failure stress and failure strain of the armchair DWBeONTs increased slightly similar to what we had already observed for Young's modulus of this chirality. Besides, a snapshot of the failure process of zigzag (8,0)@(14,0) structure is presented in Fig. 9. This figure demonstrates that the failure of the double-walled structure which started from the inner layer occurred at the same length increment compared to single-walled one (19% against 19%) and the inner layer failed sooner than the outer one.

Table 5
Mechanical properties of zigzag DWBeONTs under uniaxial tensile tests at 300°K.

Chirality	(8,0)@(14,0)	(8,0)@(15,0)	(8,0)@(16,0)	(8,0)@(18,0)
Young's Modulus (GPa)	649.69	659.75	643.97	629.19
Failure Stress (GPa)	83.36	83.96	83.74	85.31
Failure Strain	0.191	0.188	0.189	0.194

Table 6
Mechanical properties of armchair DWBeONTs under uniaxial tensile tests at 300°K.

Chirality	(4,4)@(8,8)	(4,4)@(9,9)	(4,4)@(10,10)
Young's Modulus (GPa)	636.12	638.67	640.67
Failure Stress (GPa)	101.59	102.98	103.46
Failure Strain	0.250	0.250	0.251

1.2. Mechanical properties of triple-walled BeONTs

To study more about the effect of adding walls on the properties of nanotubes, a triple-walled (8,0)@(14,0)@(20,0) zigzag BeONT and a triple-walled (4,4)@(8,8)@(12,12) armchair BeONT were simulated using MD as seen in Fig. 10. By putting both samples under uniaxial tensile loading we obtained the values of Young's modulus equal to 668.04GPa and 647.57GPa for zigzag and armchair TWBeONTs respectively shown in Table 7. These results are in agreement with those of single-walled and double-walled results which had demonstrated higher modulus for the zigzag BeONTs compared to armchair ones. Similarly, failure properties of the armchair TWBeONTs were higher than those of zigzag ones similar to what we had already found in SWBeONTs (see Fig. 4). The variation of Young's modulus with adding walls is displayed in Fig. 11. This figure confirms that with raising the number of walls from one to two and then three Young's modulus of both chirality's increased slightly so adding walls could result in nanotubes with better mechanical properties.

Table 7
Mechanical properties of zigzag and armchair TWBeONTs under uniaxial tensile tests at 300°K.

Chirality	(8,0)@(14,0)@(20,0)	(4,4)@(8,8)@(12,12)
Young's Modulus (GPa)	668.04	647.57
Failure Stress (GPa)	96.26	102.41
Failure Strain	0.22	0.24

4. Conclusion

In this article, we considered the mechanical properties of single, double and triple-walled Beryllium-oxide nanotubes (BeONTs) using molecular dynamic (MD) simulation. After putting all simulated zigzag and armchair samples under uniaxial tensile loading we found that Young's modulus of single-walled BeONTs decreased via increase in radius as well as temperature so that the highest obtained values of this property occurred in the zigzag structure (8,0) and armchair structure (4,4) with the magnitudes of 645.71GPa and 624.81GPa respectively and Young's modulus of the zigzag SWBeONTS were higher than those of armchair ones. In terms of failure properties, an increase in the diameter made no meaningful trend on the failure stress and failure strain of the SWBeONTs while temperature growing dwindled these properties for bot chirality's slightly. Unlike Young's modulus, failure properties of the armchair structure were better than those of zigzag structures. Furthermore, concerning the modulus of DWBeONTs, an interlayer distance increment resulted in Young's modulus reduction as same as SWBeONTs. Moreover, adding another wall to double-walled BeONTs improved young's modulus of both chirality's so that, the modulus of the triple-walled structures (8,0)@(14,0)@(20,0) and (4,4)@(8,8)@(12,12) with the corresponding magnitudes of 668.04GPa and 647.57GPa were higher than those of DWBeONTs (8,0)@(14,0) and (4,4)@(8,8) with the values of 649.69GPA and 636.12GPa as well as SWBeONTs (8,0) and (4,4) with the magnitudes of 645.71GPa and 624.81GPa respectively.

Declarations

Funding: No funding was received.

Conflicts of interest/Competing interests: The authors declare no competing interests.

Availability of data and material: Available by the corresponding author per request through the email (amin.hamed.m@gmail.com)

Code availability: Available by the corresponding author per request through the email (amin.hamed.m@gmail.com)

Authors' contributions: Navid Shahab analyzed the data, discussed the results, and designed the figures and tables. Yasser Rostamiyan analyzed and rechecked the results for correctness and wrote the original draft of

the article. Amin Hamed Mashhadzadeh designed the case study, wrote the LAMMPS code of the present article, and carried out the computational measurements. All authors have read and agreed to the published version of the manuscript.

References

1. Samadipakchin P, Mortaheb HR, Zolfaghari A (2017) ZnO nanotubes: Preparation and photocatalytic performance evaluation. J Photochem Photobiol A 337:91–99
2. Marana NL et al (2018) Computational simulations of ZnO@GaN and GaN@ZnO core@shell nanotubes. J Solid State Chem 266:217–225
3. Nia BA, Shahrokhi M (2018) Dilute magnetic semiconductor and half-metal behaviors in C-codoped BeO nanotubes: A first principles simulations. Chin J Phys 56(6):3039–3045
4. Kim DE, Pak D (2019) *Ti plate with TiO2 nanotube arrays as a novel cathode for nitrate reduction*.Chemosphere,
5. Taguchi T et al (2005) Synthesis of Silicon Carbide Nanotubes. J Am Ceram Soc 88(2):459–461
6. Krause M et al (2011) *High resolution TEM study of WS2 nanotubes*. Vol. 248. 2716–2719
7. Jiang Z et al (2005) GeO2 nanotubes and nanorods synthesized by vapor phase reactions. Mater Lett 59(4):416–419
8. Ganji M, Sharifi N, Ahangari MG (2014) Adsorption of H2S molecules on non-carbonic and decorated carbonic graphenes: A van der Waals density functional study. Comput Mater Sci 92:127–134
9. Ahangari MG et al (2013) Electronic and mechanical properties of single-walled carbon nanotubes interacting with epoxy: A DFT study. Physica E 48:148–156
10. Hao J-H et al (2015) An ab initio study of the size-dependent mechanical behavior of single-walled AlN nanotubes. Solid State Sci 45:30–34
11. Cong Z, Lee S (2018) Study of mechanical behavior of BNNT-reinforced aluminum composites using molecular dynamics simulations. Compos Struct 194:80–86
12. Liu X, Cheng D, Cao D (2009) The structure, energetics and thermal evolution of SiGe nanotubes. Nanotechnology 20(31):315705
13. Hamed Mashhadzadeh A et al (2018) DFT study of Ni, Cu, Cd and Ag heavy metal atom adsorption onto the surface of the zinc-oxide nanotube and zinc-oxide graphene-like structure. Mater Chem Phys 220:366–373
14. Continenza A, Wentzcovitch R, Freeman AJ (1990) *Theoretical investigation of graphitic BeO*. Vol. 41. 3540–3544
15. Hamed Mashhadzadeh A et al (2019) Theoretical studies on the mechanical and electronic properties of 2D and 3D structures of Beryllium-Oxide graphene and graphene nanobud. Appl Surf Sci 476:36–48
16. Zarghami Dehaghani M et al (2020) Fracture toughness and crack propagation behavior of nanoscale beryllium oxide graphene-like structures: A molecular dynamics simulation analysis. Eng Fract Mech 235:107194

17. Zarghami Dehaghani M et al (2021) Fracture mechanics of polycrystalline beryllium oxide nanosheets: A theoretical basis. Eng Fract Mech 244:107552
18. Rostamiyan Y, Mohammadi V, Hamed Mashhadzadeh A (2020) Mechanical, electronic and stability properties of multi-walled beryllium oxide nanotubes and nanopeapods: a density functional theory study. J Mol Model 26(4):76
19. Sorokin P, Fedorov A, Chernozatonskii L (2006) *Structure and properties of BeO nanotubes*. Vol. 48. 398–401
20. Fathalian A, Kanjouri F, Jalilian J (2013) BeO nanotube bundle as a gas sensor. Superlattices Microstruct 60:291–299
21. Chigo Anota E, Cocoletzi GH (2013) Electronic properties of functionalized (5,5) beryllium oxide nanotubes. J Mol Graph Model 42:115–119
22. Fereidoon A et al (2015) Atomistic simulations on the influence of diameter, number of walls, interlayer distance and temperature on the mechanical properties of BNNTs. Superlattices Microstruct 86:126–133
23. Bevilacqua AC, Rupp CJ, Baierle RJ (2016) First principles study on defectives BN nanotubes for water splitting and hydrogen storage. Chem Phys Lett 653:161–166
24. Yang L, Greenfeld I, Wagner HD (2016) Toughness of carbon nanotubes conforms to classic fracture mechanics. Sci Adv 2(2):e1500969
25. Zarghami Dehaghani M et al (2021) Fracture behavior of SiGe nanosheets: Mechanics of monocrystalline vs. polycrystalline structure. Eng Fract Mech 251:107782
26. Salmankhani A et al (2021) A theoretical scenario for the mechanical failure of boron carbide nanotubes. Comput Mater Sci 186:110022
27. Memarian F et al (2017) Molecular dynamic study of mechanical properties of single/double wall SiCNTs: Consideration temperature, diameter and interlayer distance. Vacuum 139:93–100
28. Zhang Y, Huang H (2008) Stability of single-wall silicon carbide nanotubes – molecular dynamics simulations. Comput Mater Sci 43(4):664–669
29. Grindon C et al (2004) *Large-scale molecular dynamics simulation of DNA: Implementation and validation of the AMBER98 force field in LAMMPS*. Vol. 362.1373–86
30. Tersoff J (1988) New empirical approach for the structure and energy of covalent systems. Phys Rev B 37(12):6991–7000
31. Cumings J, Zettl A (2000) Mass-production of boron nitride double-wall nanotubes and nanococoons. Chem Phys Lett 316(3):211–216
32. Barick A, Tripathy D (2011) *Effect of organically modified layered silicate nanoclay on the dynamic viscoelastic properties of thermoplastic polyurethane nanocomposites*. Vol. 52.312–321
33. Jalilian J, Safari M, Naderizadeh S (2016) Buckling effects on electronic and optical properties of BeO monolayer: First principles study. Comput Mater Sci 117:120–126
34. Sherafati M et al (2018) Beryllium oxide (BeO) nanotube provides excellent surface towards adenine adsorption: A dispersion-corrected DFT study in gas and water phases. Curr Appl Phys 18(9):1059–1065
35. Rastegar SF, Ahmadi A, Peyghan, Soleymanabadi H (2015) Ab initio studies of the interaction of formaldehyde with beryllium oxide nanotube. Physica E 68:22–27

36. Shahrokhi M, Leonard C (2016) Quasi-particle energies and optical excitations of wurtzite BeO and its nanosheet. J Alloys Compd 682:254–262
37. Setoodeh A, Attariani H, Jahanshahi M (2011) Mechanical Properties of Silicon-Germanium Nanotubes under Tensile and Compressive Loadings. J Nano Res 15:105–114

Figures

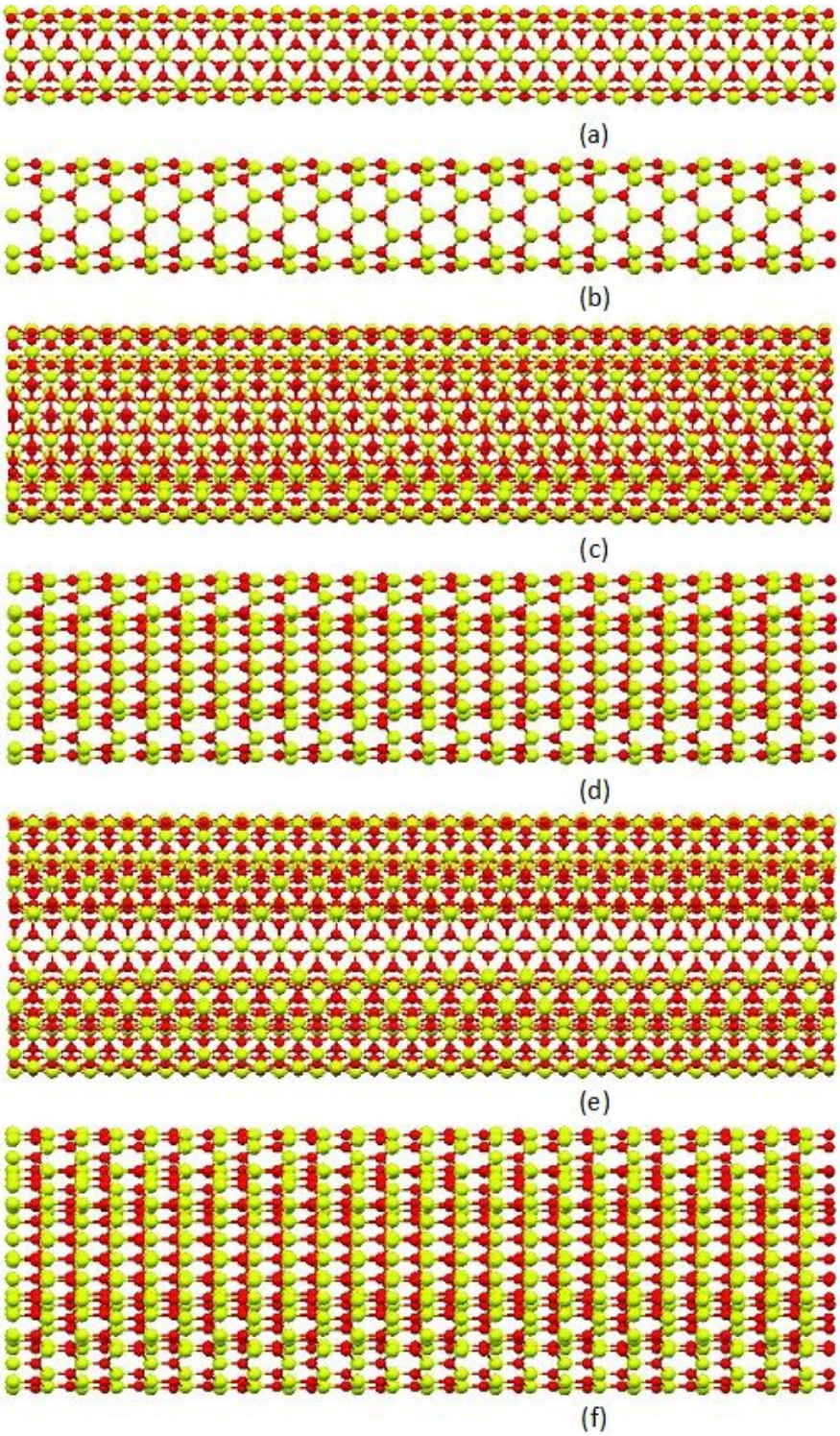

Figure 1

The structure of BeONTs (a) armchair SWBeONT, (b) zigzag SWBeONT, (c) armchair DWBeONT, (d) zigzag DWBeONT, (e) armchair TWBeONT and (f) zigzag TWBeONT

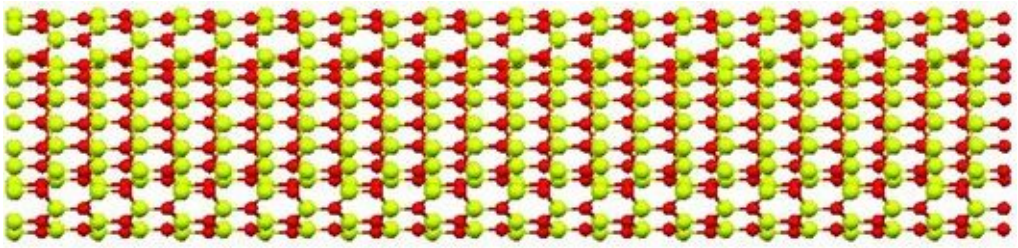

Figure 2

Tensile loaading on BeONT along x-axis.

Figure 3

(a) Stress-strain curves of zigzag SWBeONT (8,0) and (b) The second order polynomial section of Stress-strain curves of zigzag SWBeONT (8,0) at 300°K.

Figure 4

(a) young's modulus, (b) failure stress and (c) failure strain of SWBeONTs under uniaxial tensile test at 300 °K.

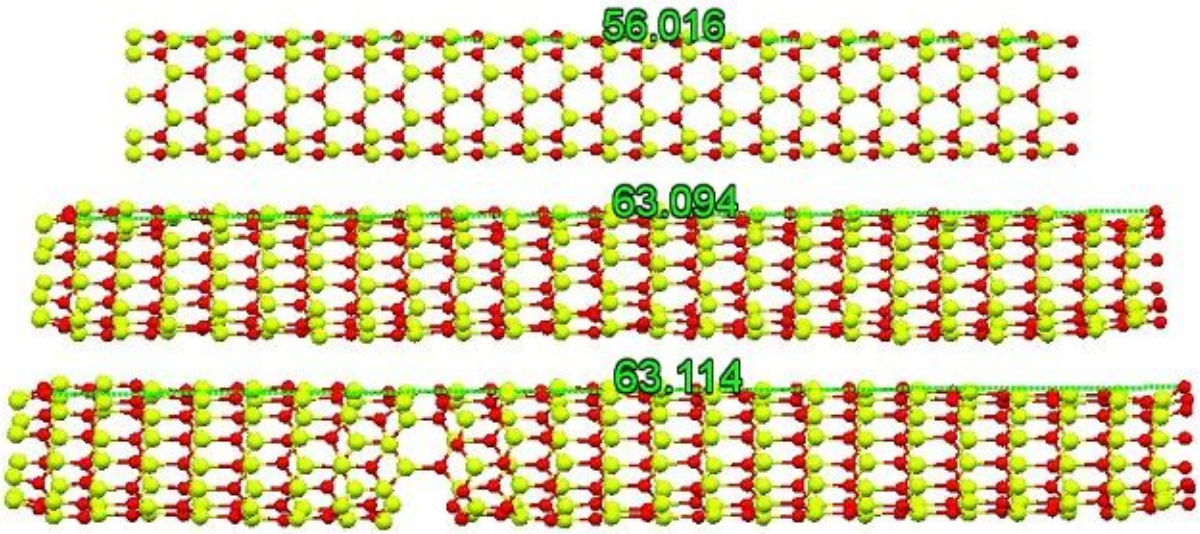

Figure 5

Snapshots of a continuous zigzag SWBeONT (8,0) failing under tensile loading condition at 300°K (unit in Angstrom for length).

Figure 6

Effect of temperature on (a) young's modulus, (b) failure stress and (c) failure strain of SWBeONT zigzag (18,0) and armchair (10,10) under uniaxial tensile test.

Figure 7

The schematics of DWBeONTs (a) (8,0)@(14,0), (b) (8,0)@(15,0), (c) (8,0)@(16,0), (d) (8,0)@(18,0), (e) (4,4)@(8,8), (f) (4,4)@(9,9) and (g) (4,4)@(10,10).

Figure 8

Obtained Young's Modulus versus interlayer distance for DWBeONTs.

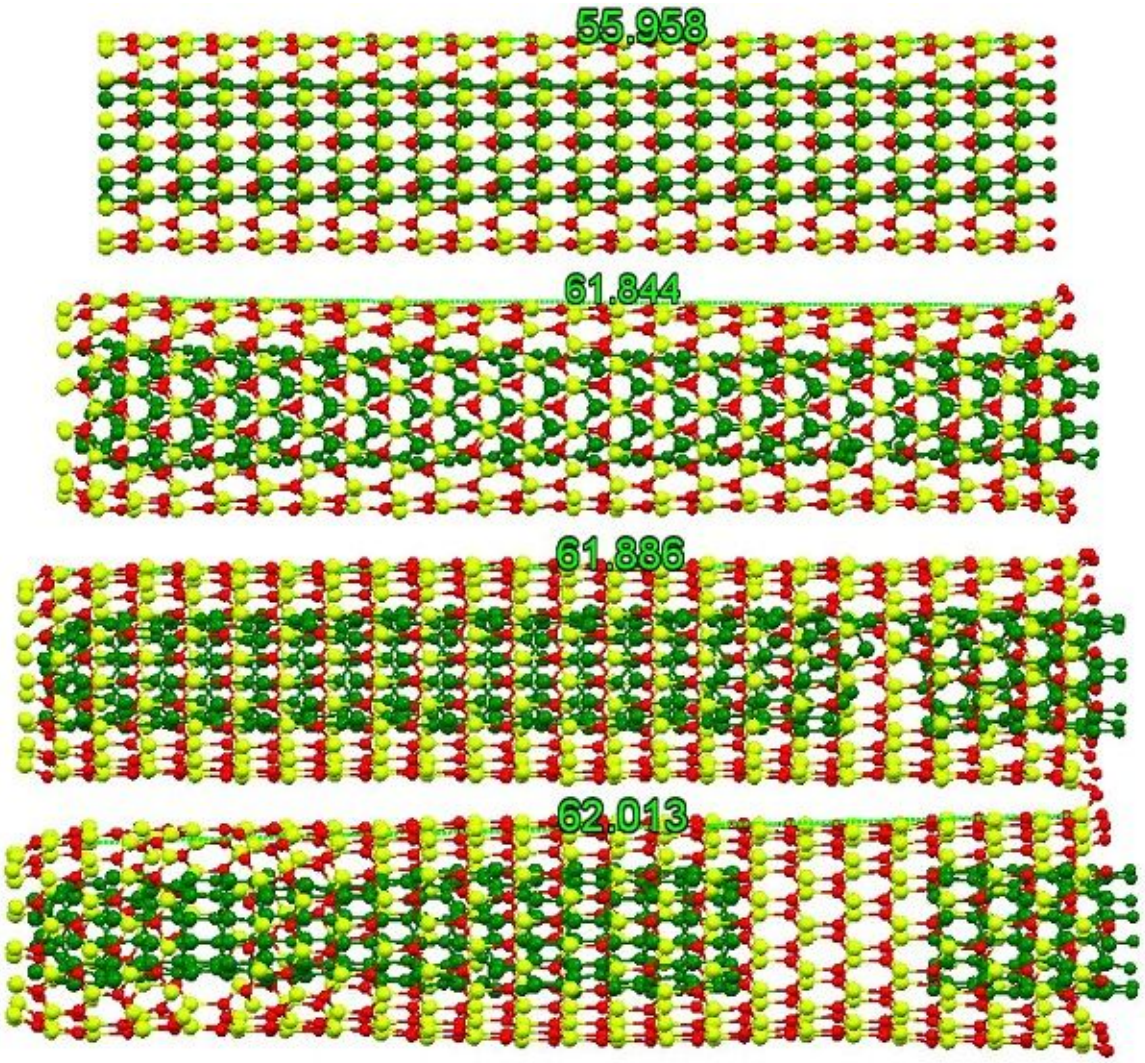

Figure 9: Snapshots of a continuous zigzag DWBeONT (8,0)@(14,0) failing under tensile loading condition at 300°K (unit in Angstrom for length).

Figure 9

Snapshots of a continuous zigzag DWBeONT (8,0)@(14,0) failing under tensile loading condition at 300°K (unit in Angstrom for length).

Figure 10

The schematics of TWBeONTs (a) zigzag (8,0)@(14,0)@(20,0) and (b) armchair (4,4)@(8,8)@(10,10) with different interlayer distance (unit in Angstrom for length).

Figure 11

The Young’s modulus as a function of diameter for different chiral types of single, double and triple-walled BeO nanotubes.